ARTICLE NO. 78-1200R

Experimental and Computational Investigation of a Swept-Wing Flow at Subsonic Speeds

A. Bertelrud*
NASA Ames Research Center, Moffett Field, Calif.

The paper reports on an experimental and computational investigation of the flow on a portion of an aircraft swept wing in a wind tunnel at low speeds. The range of angle of attack covered the domain encountered by the aircraft, and the actual outer part of a wing was used for the tests. The experiments included static pressure distributions in the leading-edge region, as well as the rest of the chord; shear-stress measurements in the leading-edge region, obtained with heated film gages; and skin-friction measurements on the main part of the wing, obtained with modified Preston tubes. Velocity profile data across the boundary layer were taken in a smaller region, and some measurements of the turbulence characteristics at a few locations on the main wing were also taken. The pressure distribution was shown to be satisfactorily represented by patching a two-dimensional inviscid method in the leading-edge region and a three-dimensional panel method on the main wing. Starting from this, boundary-layer calculations were performed with Bradshaw's finite-difference program for straight-tapered swept wings, where different spanwise stations were calculated separately. The results are encouraging, as the estimated skin-friction magnitude and trends with Reynolds numbers were predicted reasonably well.

Nomenclature

A = law-of-the-wall constant
b = span of aircraft
B = law-of-the-wall constant, half-span of wing tip tested
c = local chord
C_f = local skin-friction coefficient scaled on local conditions, $\tau/(\rho/2)U_e^2$
C_F = local skin-friction coefficient scaled on reference conditions, $\tau/(\rho/2)U_{\text{ref}}^2$
C_p = static pressure coefficient, $(p-p_\infty)/[(\rho/2)U_{\text{ref}}^2]$
D = diameter of tube
H = shape parameter, δ^*/θ
M = Mach number
p = pressure
p_∞ = pressure, undisturbed
r_0 = distance to pole
Ra = root mean square of roughness
Re/m = unit Reynolds number U_{ref}/ν
R_y = Reynolds numbers, $u_e y/\nu$
S = distance, normal to the leading edge along the surface
u^+ = parameter in the law of the wall, u/u_τ
u_τ = friction velocity, $(\tau/\rho)^{1/2}$
U,u = velocity
$\bar{U}$ = velocity vector
U_e, W_e = velocity components (freestream) normal to and parallel to the leading edge
U_{ref}, U_∞ = reference velocity, undisturbed
x = distance along chord from the leading edge
x_0 = reference length for initial conditions
$\bar{X}$ = coordinate, wing geometry
y = wall distance
y^+ = law-of-the-wall parameter, $u_\tau y/\nu$
$\bar{Y}$ = coordinate, wing geometry
α = angle of attack including tunnel corrections
α_{ind} = geometrical angle of attack
β = flow direction relative to coordinate system on the leading edge
Δp^* = differential pressure read by total head/static probes
δ^* = displacement thickness $\int_0^\delta [1-(U/U_e)]\,dy$
η = parameter for use in inverted Clauser chart, $\log(Uy/\nu)$
θ = momentum thickness, $\int_0^\delta U/U_e[1-(U/U_e)]\,dy$
θ_s = initial value of the momentum thickness
ρ = density
τ, τ_w = wall shear stress
ν = kinematic viscosity

Presented as Paper 78-1200 at the AIAA 11th Fluid and Plasma Dynamics Conference, Seattle, Wash., July 10-12, 1978; submitted Aug. 18, 1978; revision received April 5, 1979.

Index categories: Boundary Layers and Convective Heat Transfer—Turbulent; Computational Methods; Subsonic Flow.

*NRC Research Associate. On leave of absence from the Aeronautical Research Institute of Sweden. Member AIAA.

Introduction

ONE of the main problems in aerodynamics is the extrapolation of wind-tunnel model tests to full-scale conditions, normally spoken of as Reynolds number extrapolation. In a nonpressurized tunnel, one may have Reynolds numbers that are one order of magnitude less than the actual flight values. In most cases, the primary concern is for the overall forces and moments, since detailed flow investigations tend to be at a Reynolds number that is too low and a boundary layer that is too thin to be of direct use for comparisons with flight data.

The present investigation took a somewhat different approach. Instead of using a scaled-down aircraft model, the outer part of the swept wing from an aircraft was actually taken and tested in the wind tunnel. This approach was considered acceptable because the stall fence used on the aircraft could also be used in the tunnel tests and would provide starting conditions for the leading-edge flow. Preliminary wind-tunnel tests also confirmed that, for the outer portion of the wing, the general flow with respect to three-dimensionality and separation was comparable to the flight conditions.

In both the wind-tunnel tests and the flight tests, preliminary investigations were undertaken to ascertain the general flow, obtain a limited a set of data, and check out the applicability of the experimental and computational methods. Tunnel interference effects were also examined, and the relevant results are given in the present paper.

The general results[1,2] from the main wind tunnel tests and the preliminary tests[3] have been reported. The present paper selects results from all three publications and emphasizes certain aspects of the comparisons with computations. Not all data from the wind-tunnel tests have been analyzed fully yet; this is particularly true for the turbulence measurements.

Experiments

Figure 1 shows the wing, its relative size on the aircraft, and how it was mounted in the wind tunnel. The wing region tested had an NACA 64 A010 profile normal to the 25% chord line, a leading-edge sweep of 38.9%, a half-span of 2.13 m, and a taper ratio of 0.607. The experiments were performed in the 3.6-m low-speed wind tunnel of Flygtekniska Försöksanstalten (FFA) in Sweden. In the preliminary tests,[3] the angle-of-attack range varied from 0-12 deg. In the main tests, only three angles of attack were investigated—each representative of different types of flow on the wing. Table 1 gives, for each flow type, the geometrical angle of attack α_{ind}, the angle of attack after tunnel interference corrections α, the range of reference speeds U_{ref}, and the unit Reynolds number, Re/m.

The three flow types in Table 1 are comparable to conditions encountered in flight and correspond to a 1-g low-cruise speed ($M=0.4$) trajectory and landing, respectively. The Reynolds number range for the experiments at angle of attack was 1.4-5.5 $\times$ 10^6 (based on the average chord of the wing region tested). The maximum value was about one-half of the flight Reynolds number; the lowest value was comparable to that for low-speed wind-tunnel model tests.

The experiments consisted of detailed surface measurements and boundary-layer surveys. The flowfield was visualized by using an oil flow on the wing surface and using smoke in the outer flow. Static pressures were obtained from pressure taps in the surface, as well as from surveys using total head/static probes[4] on the surface. One part of the nose (approximately midway between root and tip) was instrumented with pressure taps in two rows and flush-mounted heated film gages.[5] On the main part of the wing, local skin friction and static pressure were measured with total head/static probes. Over a somewhat smaller region of the wing, total pressure rakes (with reference static pressures on) were used to measure the resultant, time-averaged, boundary-layer profiles. The use of total pressure rakes and total head/static probes was justified during the preliminary investigations of the flowfield, because the curvature of the wall streamlines, deduced from the oil flow visualizations, was rather small over the main part of the wing. Also, calculation of the outer, inviscid flowfield indicated small skewing angles (less than 10 deg) through the boundary layer; hence, the simplified techniques were assumed to be applicable.

Table 1 Flow types at various reference conditions

α_{ind}, deg	α, deg	U_{ref}, m/s	Re/m $\times 10^{-5}$	Flow type
0	0	10-50	6.8-34.2	Gradual, wedge-type transition on large part of the chord
4	4.8	10-40	6.8-27.4	Natural transition on short fraction of chord
12	14.4	10-40	6.8-27.4	Bubble transition

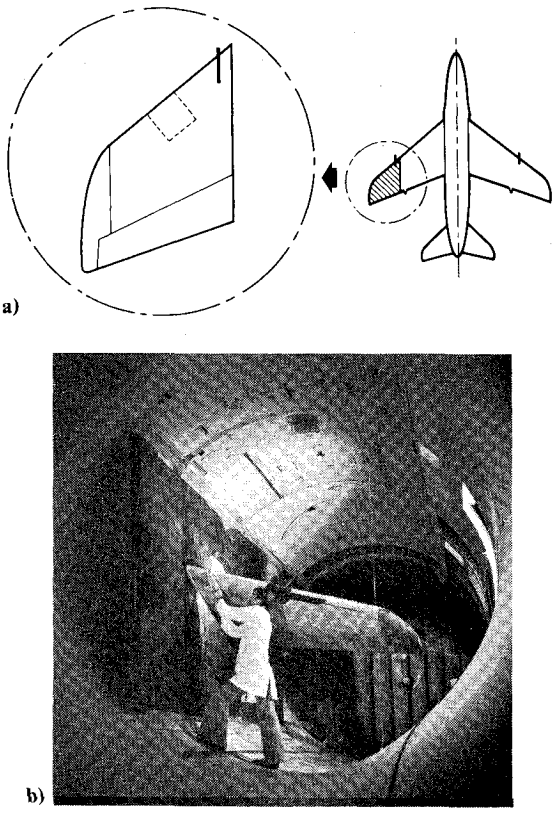

Fig. 1 Wing tip used in the experiments: a) Wing tip tested in wind tunnel and its relative size on the aircraft. (Profile: NACA 64A010 normal to the 25% chord line; leading-edge sweep: 39 deg; SAAB 32 Lansen: span = 13 m, S_{ref} = 37.4 m^2, and taper ratio = 0.375; wing tip tested: half-span = 2.13 m, S_{ref} = 4.0 m^2, and taper ratio = 0.607); b) Photograph showing the wing tip mounted in the low-speed wind tunnel.

At a few positions, a split-film probe was used to measure the instantaneous, three-dimensional velocity vector. These data have been analyzed to a limited extent, but are not included here. Also, at positions ahead of the 10% chord location, a single hot wire was used to obtain qualitative and very approximate quantitative results. These data can be found in separate publications.[1,2]

The data were recorded on the normal wind-tunnel data acquisition system; in certain check cases they were read directly from voltmeters or the anemometers. Most of the data were also recorded on 14-channel analog tape, which will be the main source for future analysis.

In most cases, measurements were obtained at three or four Reynolds numbers, corresponding to wind-tunnel reference speeds of U_{ref} = 10, 20, 30, and 40 m/s. Results from the following measurement techniques are presented in this paper:

1) Static pressures, taken from pressure taps in the surface.
2) Local skin friction, taken from total head/static probes.
3) Local skin friction, momentum thickness, shape factor, etc., taken from the total head rakes.

Data Reduction

Total Head/Static Probes

A Preston tube that sensed the total pressure at the wall was modified so that the static pressure was measured on the tube itself five tube diameters downstream of the frontal opening. Analogous to a Prandtl tube in outer flow, this technique yields a static pressure with a position error that can be accounted for. The formula used in the present evaluation was presented in Ref. 4.

$$\Delta p^*/\tau = 38.85 \log_{10}(\Delta p^* D^2/\rho\nu^2) - 107.3 \qquad (1)$$

where Δp^* is the measured differential pressure and D the tube diameter. A rough estimation of the pressure gradient effects on the readings resulting from the streamwise distance between the total head reading (at the tube front) and the

static pressure reading (5 diam downstream) can be used to correct the results, but in the present case the effects were found to be negligible and the correction has not been applied.

The measurements were performed simultaneously with six to seven probes of 2-mm diam taped onto the wing surface at positions corresponding to a specified percentage of chord and span. The probes were positioned so as not to disturb each other, and the layout of the probes insured that the probe tip could be kept at the convex surface, as is essential when using Preston tubes.

Total Head Rakes

From the readings of total pressure and corresponding static pressure, the velocity was determined, assuming that the flow was incompressible at the appropriate temperature and reference pressure. The readings were treated as if they were taken in a two-dimensional flow, and the displacement thickness, momentum thickness, etc., were deduced by means of two-dimensional formulae.

The skin friction was originally reduced by many different methods.[1,2] In the present paper, only the results from the Clauser chart method are given. At each point in the profile, an equivalent skin friction was determined by use of an expression obtained by direct inversion of a Clauser chart:

$$C_f = 2(y^+/R_y)^2 \tag{2a}$$

where

$$y^+ = 10^{(-0.523439+0.677334\eta+0.0418185\eta^2-0.00248291\eta^3)} \tag{2b}$$

and

$$\eta = \log 10(Uy/\nu) \tag{2c}$$

The numerical values given are valid for Coles' values of the law-of-the-wall constants:

$$\begin{aligned} u^+ &= A\log_{10}y^+ + B \\ A &= 5.62 \\ B &= 5.0 \end{aligned} \tag{3}$$

The actual values of the skin-friction coefficients were then determined as the average of the values from Eqs. (2) using data from locations below a tenth of the boundary-layer thickness. Since the surface of the wing was convex, the first measurement point was located a small distance above the surface. The magnitude of this distance was measured with a thin metal strip.

Computations

The inviscid flow close to the leading edge was estimated with a two-dimensional method.[6] The flow was considered to consist of a flow normal and parallel to the leading edge. The flow normal to the leading edge was calculated with the two-dimensional method using, as an angle of attack, $\alpha_{2\text{-D}} = \alpha \times \cos(38.9\text{ deg})$. The static pressure was determined by assuming an infinite swept wing with a spanwise flow component of $W_e = (U_{\text{ref}})(\sin 38.9\text{ deg})$.

From the calculated inviscid flow components U_e/U_{ref} and W_e/U_{ref}, the boundary-layer development in the nose region was calculated by means of a simple integral method.[7] According to the independence principle for laminar boundary layers, the crosswise viscous flow can be calculated independently of the spanwise flow. Thus, the Thwaites' method was used for this component and the spanwise boundary layer was computed as a constant pressure layer. This approach gave indications of separation that should be correct, but did not give indications of crossflow instability, since the flow at the suction peak would always be predicted as collateral.

On the main portion of the wing, a panel method[8] was used to calculate the inviscid flowfield. The panels were distributed evenly in the spanwise direction. The panels were flat, and the boundary conditions were fulfilled at the wing surface. Figure 2 shows the panel distribution relative to the size and shape of the experimental wing. The wing tip was modeled crudely, as it was considered more important to pick up spanwise variations further inward. Close to the leading edge, the panels would not properly represent the wing; therefore, it was assumed that the panel solution could be patched to the two-dimensional solution extended to infinite swept-wing conditions.

Starting with the calculated pressure distribution, the turbulent boundary layer on the main portion of the wing was predicted with Bradshaw's finite-difference computer code for straight-tapered swept wings.[9] The assumption was that the isobars were straight and had a center, which, in the present case, was assumed to coincide with the center of the generators. The calculation used the geometry in Fig. 3 along a periphery going through the 25% chord line at the proper spanwise station. The pressure distribution was input at 21 equidistant points covering the wing.

One of the basic difficulties in the turbulent boundary-layer calculations was the prescription of initial conditions. The laminar boundary-layer program[7] could give the separation rather accurately, but a constant pressure assumption over the laminar part of the separation bubble was found to be unrealistic. Van Ingen[10] calculated the equivalent two-dimensional profiles at appropriate Reynolds numbers, and, as was shown earlier,[1] both the separation point and the reattachment point were accurately predicted, indicating that the spanwise flow had a small influence. The pressure distribution was also well predicted, with a significant pressure rise under the laminar part of the shear layer and a much steeper rise under the turbulent layer. However, this did

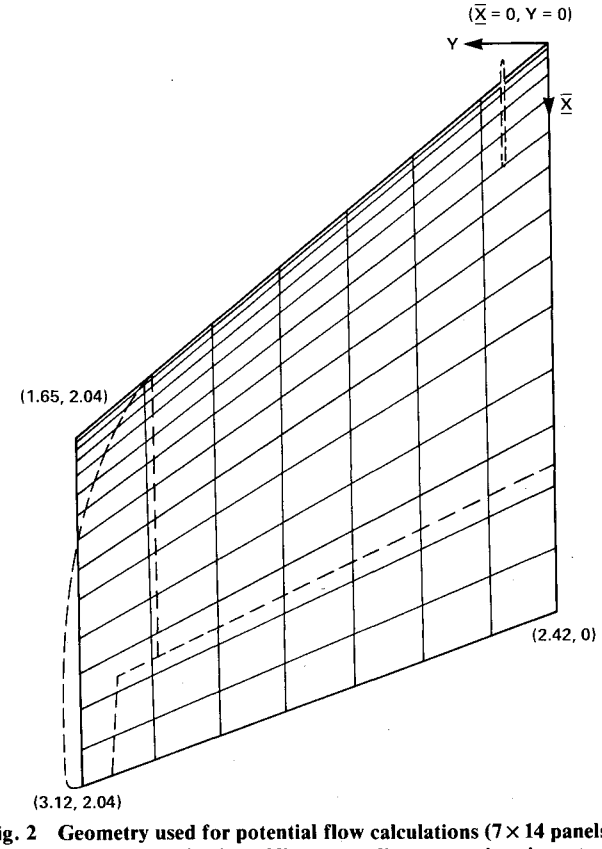

Fig. 2 Geometry used for potential flow calculations (7 × 14 panels). Real wing is indicated by dotted lines; coordinates are given in meters.

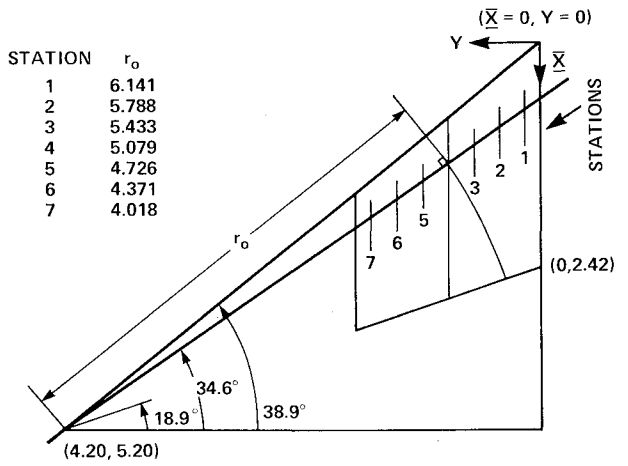

Fig. 3 Wing geometry used for the boundary-layer calculations. Measurements are given in meters.

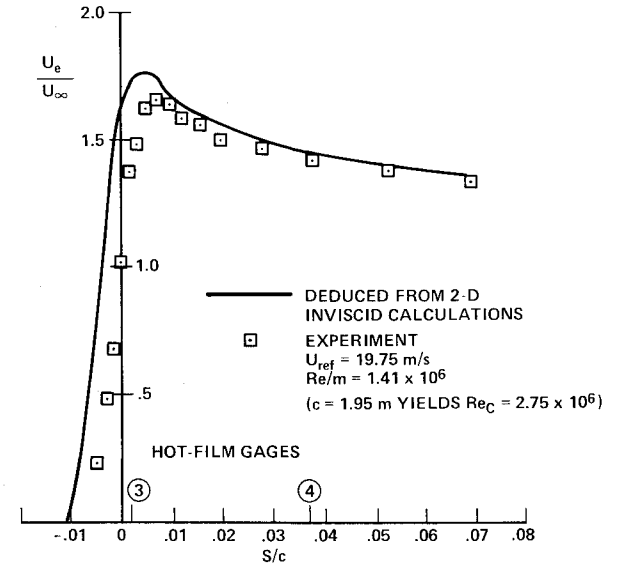

Fig. 4 Comparison between crosswise (normal to leading edge) velocity distribution U_e/U_∞ deduced from experiment and two-dimensional calculations. $\alpha = 3.73$ deg (two-dimensional) equivalent to $\alpha = 4.8$ deg for present wing tip.

not allow any firm conclusions to be drawn concerning proper starting conditions for the turbulent boundary layer. The single wire profiles taken at 3.5% chord could provide some information and give an approximate value of the initial momentum thickness, but since these measurements did not contain any information on crossflow, they were disregarded for the present. Therefore, the local outer streamline condition at the initial computation station, taken at 6% chord, was the one given by assuming infinite swept-wing flow at that position. The initial momentum thickness was determined from the formula

$$\theta_s = 0.0142(\nu/U_{\text{ref}})^{1/7} x_0^{6/7} \tag{4}$$

where x_0 = (0.1436) chord (local). Hereafter, this initial condition is referred to as the "standard" condition. In addition, computations were performed with "double" and "half" initial momentum thicknesses, thus covering the probable region of initial values.

The surface condition of the experimental wing was essentially the same as that flown on the aircraft (i.e., with camouflage paint, etc.). The *Ra* (root mean square of the roughness) was measured prior to the experiments and found

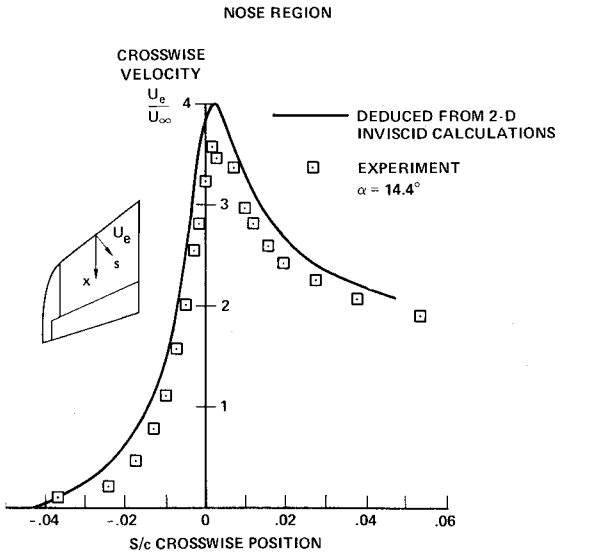

Fig. 5 Comparison between crosswise velocity distribution U_e/U_∞ deduced from experiment and two-dimensional calculations. $\alpha = 11.28$ deg (two-dimensional) equivalent to $\alpha = 14.4$ deg for present wing tip.

to be on the order of 0.5-1 μm; no measured *Ra* value exceeded 2.5 μm. The boundary-layer program[9] has an option including equivalent sand roughness. Thus, runs were made with identical initial conditions but with a roughness of 10 μm, which was representative of the worst possible roughness effect on the wing. The wing also had some rain erosion in the leading-edge region. Covering the leading-edge region with a thin, smooth mylar sheet (Monokote) demonstrated that this roughness had no effect on the flow. (This conclusion was based on both surface flow visualizations and measurements.)

In the computations, initial C_f was given as a flat-plate Spalding-Chi value and the initial profile was a two-dimensional "synthetic" one, based on a Coles' velocity profile family. The effects of assuming a collateral initial profile were explored earlier.[2] It was found that a difference of 5 deg between the outer flow direction and the shear stress direction at the wall resulted in a difference of 1 deg and less for the regions of the wing of interest for comparisons with the total head/station probe and rake results.

Results and Discussion

Static Pressure Distribution

Figures 4 and 5 show typical results for the component normal to the leading edge U_e/U_∞. The experimental points have been deduced from the measured C_p values by assuming infinite swept-wing flow:

$$U_e/U_\infty = U_e/U_{\text{ref}} = [1 - \sin^2(38.9) - C_p]^{1/2} \tag{5}$$

The two-dimensional calculations with the inviscid program[6] predicted the data in the region forward of 7% chord. Both the magnitude of the suction peak and its position were in good agreement with the experiment. The attachment line position appears correct, although it was very difficult to determine accurately from experiments, since there was a rather wide region of low-speed flow. This was particularly true for the high angle-of-attack case. This difficulty in determining the attachment line position is one of the basic points in the later discussion concerning possible attachment line transition and indications of subsequent relaminization ahead of the suction peak for the highest angle of attack.

Figure 6 shows an example of the measured pressure distribution along one chord in the form

$$(U_e^2 + W_e^2)^{1/2}/U_{\text{ref}} = (1 - C_p)^{1/2} \tag{6}$$

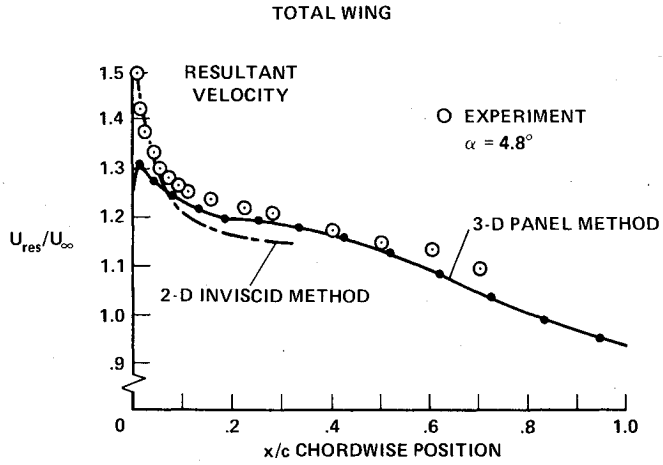

Fig. 6 Relative resultant velocity deduced from calculations for $y/B = 59\%$ (inviscid panel method) at $\alpha = 4.8$ deg.

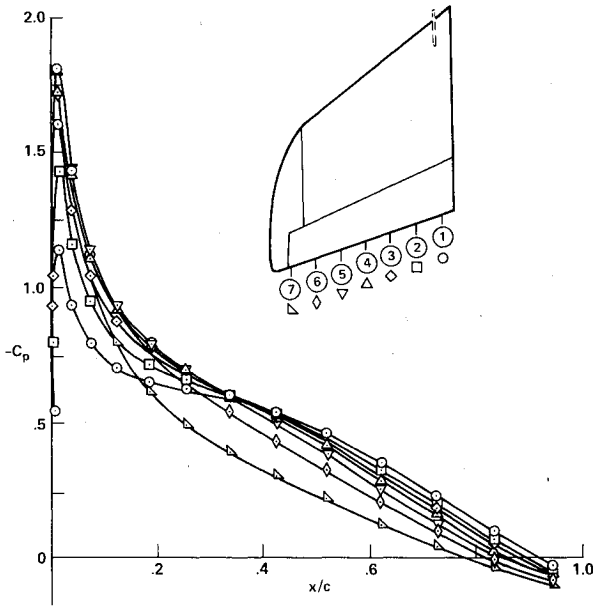

Fig. 7 Calculated pressure distribution on the suction side on the wing tip at $\alpha = 14.4$ deg for seven spanwise sections.

The results of calculations with the two-dimensional profile method and the three-dimensional panel method (both inviscid) are plotted for comparison. It can be seen that it is possible to predict the pressure distribution accurately by patching the two methods somewhere ahead of $x/c = 10\%$. The same type of patching is possible even at 14.4 deg angle of attack.

We decided to base the boundary-layer prediction on the calculated pressure distributions, since extensive measured pressure distributions were available at only one spanwise station, although some pressure taps were positioned at other stations to detect root or tip effects. We also decided to base the calculations on the pressures from the panel method to avoid the patching. Since the calculations were started at 6% chord, the difference should be very small.

Figure 7 shows the calculated pressure distributions for 14.4 deg angle of attack. Except for the two first stations at the root and the last station at the tip, the pressures varied little in the spanwise direction; the pressure gradient in the x direction was almost constant beyond 15% of the chord. The suction peak became more pronounced as one moved out toward the tip.

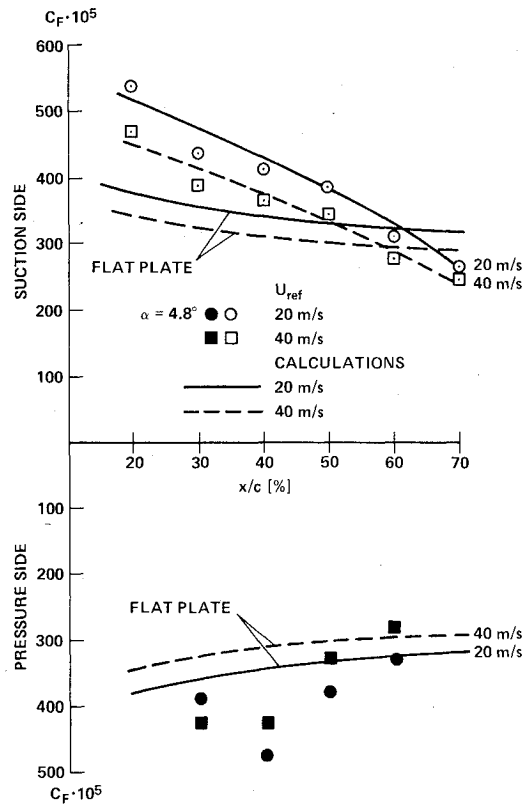

Fig. 8 Skin friction distribution in the chordwise direction from the total head/static probes. Note that here C_F is based on U_{ref}.

Viscous Flow on the Main Wing

In this section, discussion is divided into two parts, each corresponding to a different angle of attack. The results from both total head/static probes and rakes are compared with the computations.

Transition without a Separation Bubble ($\alpha = 4.8$ deg)

The total head/static probes measured the local shear stress, but, in this case, the proper scaling parameter was the flight dynamic pressure, not the local value. In Fig. 8, C_F denotes that the shear was scaled by the reference speed U_{ref}. The results are given for the 50% span stations for both the suction and pressure sides. Calculations from the three-dimensional boundary-layer code and a simple flat-plate formula, commonly used in drag prediction programs, are shown. On neither side of the wing did the simple flat-plate formula predict the measured variation along the chord. The three-dimensional boundary-layer predictions on the suction side were quite good with regard to the variation along the chord and the trends with speed (Reynolds number). The maximum skin friction indicated at $x/c = 40\%$ for the pressure side was probably an indication that transition was taking place in this vicinity.

Some attention must be given to the influence of different choices for initial values of the momentum thickness. These choices and the predictions of skin friction for actual flight conditions are treated in Figs. 9-11.

Figure 9 gives the results of doubling or halving the momentum thickness on the local skin friction. Decreasing the momentum thickness increases the skin friction, but the effect is rather small, except for a region on the forward part of the wing. If the momentum thickness were increased, however, the C_f values were lowered somewhat more than might have been expected from the former case.

The corresponding development of the momentum thickness for various assumed initial thicknesses is shown in Fig. 10. The values predicted from the standard initial con-

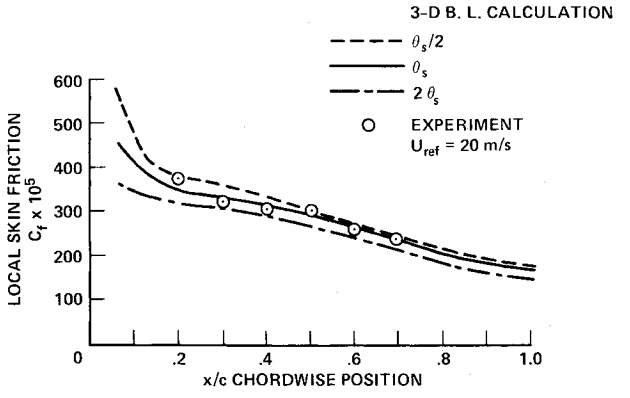

Fig. 9 The effect of initial assumed momentum thickness on the development of total skin friction C_f downstream; station four, $y/b = 50\%$, $\alpha = 4.8$ deg.

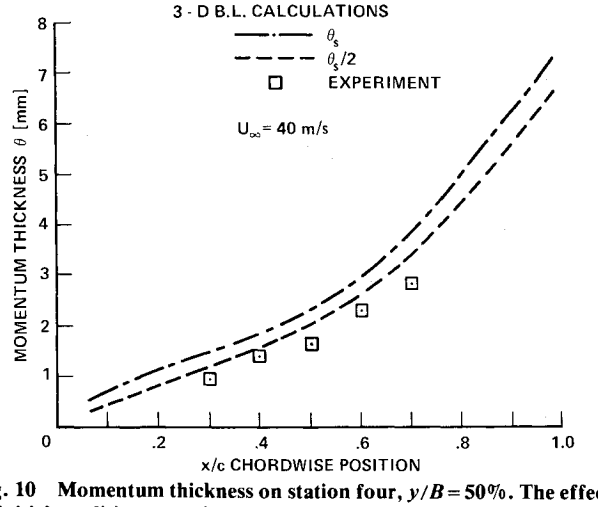

Fig. 10 Momentum thickness on station four, $y/B = 50\%$. The effect of initial conditions, $\alpha = 4.8$ deg.

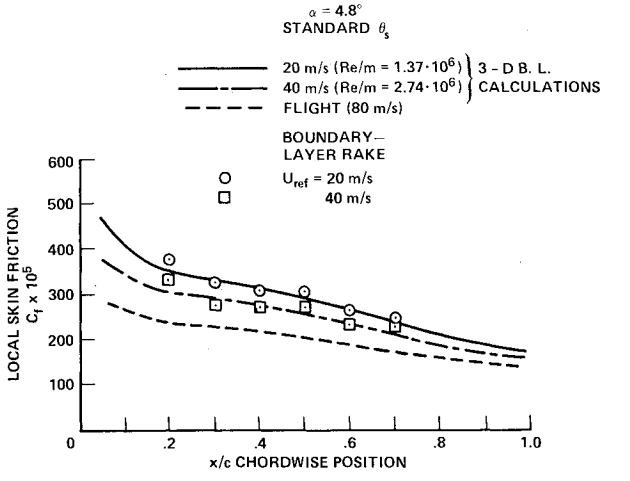

Fig. 11 Local skin friction at different Reynolds numbers, $y/b = 50\%$.

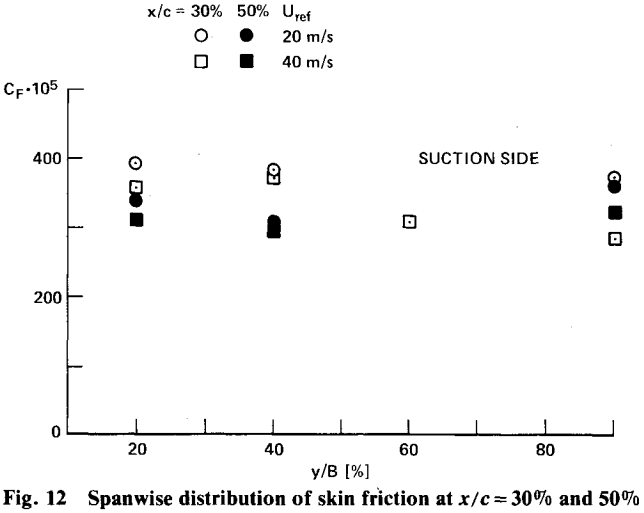

Fig. 12 Spanwise distribution of skin friction at $x/c = 30\%$ and 50% determined by total head/static probes, $\alpha = 14.4$ deg.

ditions from Eq. (4) were too high. Decreasing the standard value of θ by one-half gave better agreement with the data. Note, however, that at 10 m/s, dropping the initial thickness by one-half gave momentum thickness Reynolds numbers that were too small for a turbulent boundary layer to exist. This meant that the calculations should properly start further downstream.

Figure 11 gives the local skin friction along the chord for two different speeds tested in the tunnel, and also the flight speed corresponding to this particular angle of attack. The calculations were performed with the 10 μm sand roughness for all the cases with the standard initial values of momentum thickness. The inclusion of roughness did not influence the calculated results. The proper trends with speed were predicted and the extrapolation to the flight speed resulted in lower values of skin-friction coefficient.

Transition with a Separation ($\alpha = 14.4$ deg)

The preceding section showed that the initial momentum thickness might have a large influence; in light of this, the proper momentum thickness to use for the reattached boundary layer behind the bubble for the present test condition is unknown at this time.

Figure 12 gives the spanwise distribution of skin friction at two chordwise stations, as determined by means of the total head/static probes. The values were nearly constant in the spanwise direction. Concerning the difference between values at 30 and 50% chord, it should be noted that the difference in reference conditions (i.e., C_f vs C_F) may have a large effect.

Flow Features in the Leading-Edge Region

At low angles of attack, the investigation indicated a laminar attachment-line flow either gradually becoming transitional and turbulent in the vicinity of the leading edge, or separating and reattaching as a turbulent layer behind a short bubble. At the highest angle of attack in the present investigation $\alpha = 14.4$ deg, which corresponds to stall conditions, an interesting leading-edge flow is encountered. Figure 13 is an oil flow picture taken at 30 m/s. It shows the leading-edge region with 0.2 mm thick (grey) tape attached parallel to the leading edge. In flight it had been found that some examples of this aircraft type had unwanted stall behavior; a sudden roll and yaw motion might occur during landing. A series of flight tests showed that 0.4 mm thick tape fixed at a specific position relative to the leading edge alleviated the problem. If the tape was moved only 10 mm forward or rearward, it did not have any effect. In the tunnel tests, tape was positioned according to the specifications (B) and also 10 mm forward (A) and rearward (not shown). The oil flows substantiate the findings from the flight tests. At position A (or no tape), a separation bubble occurs behind the tape trailing edge. At position B, the tape trailing edge triggers transition and subsequent reattachment. In the third case, the separation occurred on top of the tape. This may be correlated with the pressure distributions calculated and measured in the wind tunnel, and a hypothesis for the function of the tape may be presented: tape A has its trailing edge upstream from the suction peak, i.e., the laminar layer reattaches and is ac-

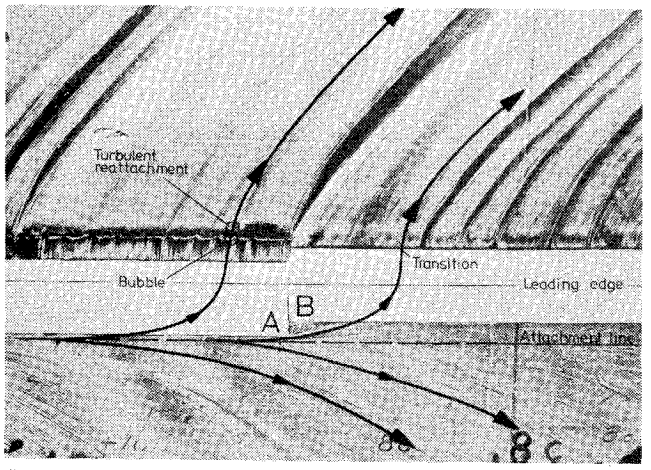

Fig. 13 Photograph showing details of the nose region flow at $\alpha = 14.4$ deg, as illustrated by means of oil flow (from Ref. 1).

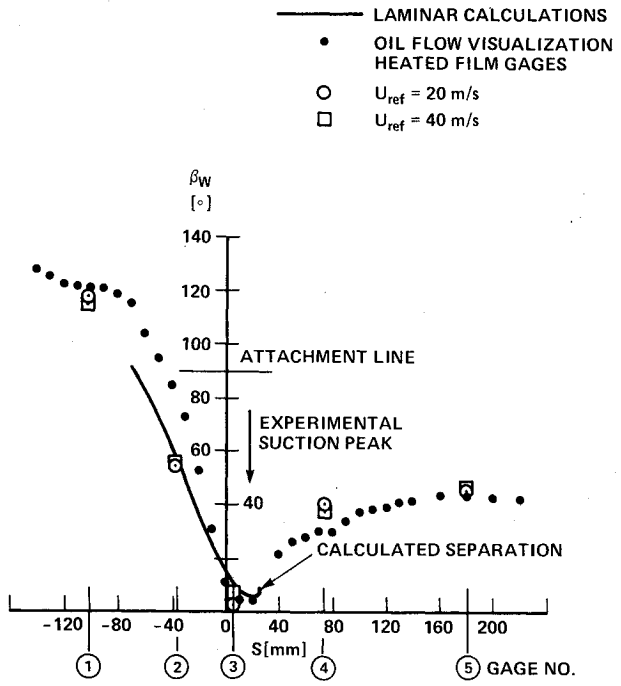

Fig. 14 Wall streamline directions at $\alpha = 14.4$ deg from measurements and calculations. The position of the suction peak for the calculations is made to correspond to the experiments.

celerating stably. The trailing edge of tape B triggers transition because it is located in between the suction peak and the separation point where the laminar boundary layer is unstable. The rear edge of tape C is located aft of the separation point, and hence has no effect.

In Fig. 14, the flow direction in the leading-edge region is shown as found from calculations, interpretations of the oil flow, and results from the skin-friction gages.

In Ref. 11 a discussion is made of the possibility of a transitional/turbulent attachment-line flow with subsequent relaminarization at this angle of attack.

Conclusions

The following main conclusions were drawn from the investigations:

1) Pressure distribution in the nose region can be treated as quasi two-dimensional (i.e., as if it were an infinite swept wing), despite the very low aspect ratio of the wing region tested. This solution then may be patched to, for example, a panel method result for the rest of the wing.

2) Total head/static tubes, i.e., modified Preston tubes, can be used to map the static pressure and skin-friction distribution over the wing, despite relatively large pressure gradients.

The calculations performed with the straight tapered swept-wing program of Bradshaw et al.[9] for the turbulent boundary layer, under the assumption of straight isobars with common intersection, gave good results for the present wing. For example: 1) the magnitude of the skin friction was predicted with good accuracy; 2) the Reynolds number effect was predicted satisfactorily; and 3) the initial value of momentum thickness may have a small influence on the predicted development of local skin friction, C_f.

Acknowledgment

This work was performed at the Aeronautical Research Institute of Sweden and was sponsored by the Defense Materiel Administration of Sweden, Air Materiel Department.

References

[1] Bertelrud, A., "Measurements on a Three-Dimensional Swept Wing at Low Speeds. Part 1. The Flow Around the Leading Edge," The Aeronautical Research Institute of Sweden, Rept. 130, 1977.

[2] Bertelrud, A., "Measurements on a Three-Dimensional Swept Wing at Low Speeds. Part 2. The Flow in the Boundary Layer on the Main Wing," The Aeronautical Research Institute of Sweden, Rept. 131, 1977.

[3] Bertelrud, A., "Wind Tunnel Measurements in the Boundary Layer on a 3-D Swept Wing," The Aeronautical Research Institute of Sweden, TN AU-1191, Dec. 1976.

[4] Bertelrud, A., "Total Head/Static Measurements of Skin Friction and Surface Pressure," *AIAA Journal*, Vol. 15, March 1977, pp. 436-438.

[5] McCroskey, W.J. and Durbin, E.J., "Flow Angle and Shear Stress Measurements Using Heated Films and Wires," *Transactions of the ASME, Journal of Basic Engineering*, Vol. 74, March 1972, pp. 46-52.

[6] Eriksson, L.-E., "Calculation of Two-Dimensional Potential Flow Wall Interference for Multi-Component Airfoils in Closed Low-Speed Wind Tunnels," The Aeronautical Research Institute of Sweden, TN AU-1116, April 1975.

[7] Bertelrud, A., "Calculation of Laminar Boundary Layers on Infinite Swept Wing Starting from Thwaites' 2-D Method," (in Swedish) The Aeronautical Research Institute of Sweden, TN AU-1431, 1977.

[8] Gustavsson, A.L. and Hedman, S.G., "An Improved Version of a Panel Method for the Prediction of Aerodynamic Characteristics of Wing-Body-Tail Combinations at Subsonic and Supersonic Speed," presented at EUROMECH 75, Braunschweig/Rhode, May 1976.

[9] Bradshaw, P., Mizner, G.A., and Unsworth, K., "Calculations of Compressible Turbulent Boundary Layers with Heat Transfer on Straight-Tapered Wings," Imperial College of Science and Technology, IC Aero Rept. 75-04, 1975.

[10] Van Ingen, F.L., "On the Calculation of Laminar Separation Bubbles in Two-Dimensional Incompressible Flow," AGARD CP 168, Paper 11, 1975.

[11] Bertelrud, A., "An Experimental and Computational Investigation of a Swept Wing Flow at Subsonic Speeds," AIAA Paper 78-1200, Seattle, Wash., July 10-12, 1978.